Multi-objective Optimization of Graft Configuration using Genetic Algorithms and Artificial Neural Network

CATARINA F. CASTRO, CARLOS C. ANTÓNIO, LUÍSA C. SOUSA
LAETA/INEGI, Engineering Faculty
Universidade do Porto
Rua Dr. Roberto Frias s/n, 4200-465 PORTO
PORTUGAL
ccastro@fe.up.pt   http://paginas.fe.up.pt/~ccastro/

Abstract: - Optimization of graft geometric configuration with regard to blood dynamics is the major target of this research. A developed multi-objective genetic algorithm is considered in order to reach optimal graft geometries for idealized arterial bypass systems of fully occluded host arteries. An artificial neural network simulating hemodynamic specific conditions is introduced in order to reduce the genetic search computational time. Input data values are constrained within pre-defined boundaries for graft geometric parameters and the correspondent target values are solutions for blood velocity and shear stress functions calculated with a finite element simulator. Optimal solutions are presented as Pareto fronts covering a range of best possible solutions.

Key-Words: - Shape optimization, Multi-objective optimization, Genetic algorithms, Artificial Neural Networks, Biomedical engineering

1 Introduction

Vascular diseases, such as severe atherosclerosis, are often life threatening diseases. In order to overcome severe vessel stenosis surgical interventions using bypass grafts are usually considered. Researchers have developed artificial graft tissue by combining man-made materials with human cells to make it elastic and durable and so it can be attached to the host artery and efficiently replace the obstructed conduct. Nevertheless, several studies have proven that restenosis phenomena develop in bypass-artery junctions leading to poor performance and failure of the surgery [1], [2]. Initiation and progress of these diseases are not fully understood but though to be a consequence of physiological response to abnormal conditions of local hemodynamics [3].

Many research projects clearly show that diseases primarily occur at regions of complex and instable blood flow. In the cardiovascular system, development of atherosclerosis disease is mainly observed in regions of transient flow reversal, typically near bifurcations and along curved vessels [3]-[5]. So, the geometric configuration of vascular bypass grafts might have a profound influence on flow patterns. Improving blood flow dynamics in the artery/graft system is an important element for long-term success of bypass surgeries.

Computational approaches have been used simulating blood flow through idealized bypass models. They exhibit particular patterns characterized by the presence of recirculation zones and secondary flows in critical regions [6]-[8]. The optimization of graft and anastomotic configurations with regard to fluid dynamics is the major target of this study. The problem is related with both optimal shape design and flow control that are involved in the simulation of the bypass system with cost functions associated to flow rate and shear stress which are thought to be correlated with occlusion pathogenesis [9].

In this project a developed multi-objective genetic algorithm is considered in order to reach optimal graft geometries for idealized arterial bypass systems of fully occluded host arteries [6], [10]-[11]. Genetic algorithms are based on Darwin's theory of population evolution [12]-[13]. Once an initial population is created, new populations are generated following the previous one according to principles of reproduction, mutation and survival of the fittest. The best design points in the population are considered to be the most fitted ones. The considered genetic algorithm (GA) supported by an elitist strategy seeks to increase fitness as it operates [6], [10]. Ultimately, the method identifies optimal solutions as a family of design points that are non-dominated till the end of a predefined number of generations.

Genetic algorithms require a large number of computer simulations. So, an artificial neural

network (ANN) is developed to efficiently simulate blood flow for specific graft geometries. Input, hidden and output layers model the topology of the ANN. The weights of the synapses and the biases for hidden and output nodes are used as design variables in the ANN learning process. Input and target data have been acquired using a finite element arterial blood simulator previously developed and tested considering fully unsteady incompressible Navier-Stokes equations and a three-dimensional geometry [6], [11], [14].

Numerical results show the important flow features, which are suspicious to relate the intimal hyperplasia in arteries with development of stenosis, flow recirculation and shear stress distributions in the graft system being influenced significantly by the bypass geometry. The benefits of numerical shape optimization in achieving design improvements before a bypass surgery, minimizing blood recirculation zones as well as low wall shear stress areas at the toe and heel of the distal anastomosis, might lead to minimization of bypass surgery failure.

2 Graft Geometry

The background provided by mathematical modeling and numerical simulation allows the use of new techniques with the aim of optimizing the (full) configuration and the (local) shape of a simplified bypass model. The present paper intends to carry out a numerical analysis on flow fields of a fully stenosed artery with a complete bypass graft implanted on it. The simplified arterial graft prosthesis is a tubular vessel disposed around a longitudinal axis as described in the bypass model given in Fig. 1. Four design variables will be considered: the distance from the near wall of the graft to the near wall of the artery H, the junction angle β, the width of the prosthesis at its longitudinal symmetric line W_p and the suture line dimension D. The host artery is assumed to be a fully stenosed conduit, simulated using two cylindrical tubes of 9 mm diameter, the proximal host artery before the obstruction and the distal host artery after obstruction. The graft is symmetric and meets the host artery with a side-to-end proximal anastomosis and an end-to-side distal anastomosis. As usually adopted by most previous investigations, vessels are assumed to be impermeable rigid tubes.

To our knowledge, most authors consider circular or polynomial symmetric geometries for the prosthesis with variable junction angles [8], [15]. Small junction angles have more obvious advantages for the hemodynamics of bypass grafts

[8], [16]. Using a circular prosthesis, the optimal limit for junction angle would be close to zero producing an extremely large graft/artery junction. Instead, this investigation will address sinusoidal geometries with graft walls being drawn by sine curves.
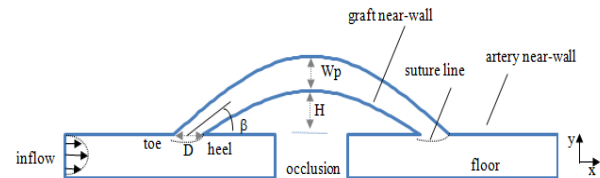

Fig.1 Anastomotic configuration and nomenclature of the graft/artery geometry

3 Bypass Hemodynamics

Improvement in the understanding of the genesis of diseases is very important as it allows the reduction of surgical and post-surgical failures. Mathematical modeling and numerical simulation of physiological flows allow a better understanding of phenomena involved in artery diseases. It may also suggest new means in bypass surgical procedures as well as with less invasive methods to devise new shapes in bypass configuration [17], [18].

The background provided by mathematical modeling and numerical simulation of blood flow has led to the application of numerical techniques for the optimization of the (full) configuration and the (local) shape of a simplified bypass model [5], [11], [19], [20]. In support to this aim at macro-geometrical level, efficient schemes are being used to provide useful and quick indications (outputs) in a repetitive design environment as shape design requires [6], [15], [16], [18].

A study of important geometrical quantities using the defined bypass geometry is described here. It considers a finite element methodology (FEM) and a previously developed and tested simulator [11], [14]. The governing equations for this problem are the Navier–Stokes set equations that consist of the continuity and the momentum equations. The hemodynamics problem is considered laminar since the anastomotic flow typically reaches a maximum Reynolds number less than 1000. The non-Newtonian rheology is accounted for through the Casson non-Newtonian model [19]. The dynamic viscosity μ is a function of the fluid shear strain rate γ [s^{-1}] and expressed as

$$\mu = 0.1\,(k_0(c) + k_1(c)\sqrt{\gamma}\,)^2/\gamma \quad [\text{Pa s}] \qquad (1)$$

with $k_0 = 0.194$ Pa$^{1/2}$ and $k_1 = 0.055$ (Pa s)$^{1/2}$ for a 45% hematocrit (c). An upper limit of shear rate was set, to limit the values of viscosity. It avoids singularities that lead to high non-physical values. Viscosity ranged from 0.004 to 0.06 [Pa.s].

Blood flow is pulsatile by nature. The arterial wall is assumed to be rigid, a pulsatile waveform is prescribed at the inlet and a no-slip condition (zero velocity) is prescribed at the walls. At the artery inlet, the velocity profile is assumed parabolic. Details on the mathematical formulation and finite element approximation are given in Sousa et al. [11], [14].

The purpose of this research is to contribute towards the improvement of longevity of arterial bypass surgeries. Poor performance and failure of arterial grafts is due to the development of anastomotic intimal hyperplasia at the host artery floor opposite to the distal anastomosis what is thought to be purely caused by fluid mechanical factors [21]. In order to understand the dependence of the blood hemodynamics on this particular graft geometry, FEM simulations were performed considering only symmetric geometries since removing the symmetry constrain does not have a significant effect [15]. Fig. 2 presents the deformable mesh considered for the FEM simulation. The model includes both the proximal and distal bypass sections in order to analyze the flow development in the entire bypass.
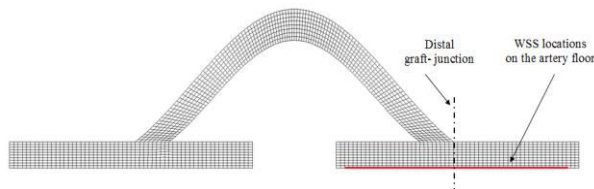

Fig. 2 Mesh for FEM simulation of simplified sinusoidal graft model

In this study, the bifurcating flow rate into bypass graft is not a concern since the fully occluded host artery is assumed and 100% flow issuing from the host artery entrance bifurcates into the bypass graft. Details on three different graft geometries are reported in Table 1 and Fig. 3 to 5.

The difference between grafts A and B is the inflow blood velocity simulating two different instants of the cardiac cycle. V_{peak} defines the maximum inflow velocity imposed at the artery inlet and V_{max} the maximum velocity reached all along system during the FEM simulation. The difference between graft B and C is the prosthesis geometry:

graft C is narrower than graft B for the same artery diameter and artery inflow.

Table 1. Geometric and velocity details of the simulated grafts

Graft	A	B	C
H [mm]	25.0	25.0	13.0
β [rad]	0.785	0.785	0.785
W_p [mm]	17.7	17.7	5.6
D [mm]	14.1	14.1	8.0
V_{peak} [mm/s]	85.	210.	210.
V_{max}/V_{peak}	1.1	1.2	1.5

Fig. 3 presents the simulated longitudinal velocity distribution for grafts A, B and C respectively. The blood flow through the idealized bypass models has a particular pattern, which is characterized by the presence of recirculation zones and secondary flows in certain regions.
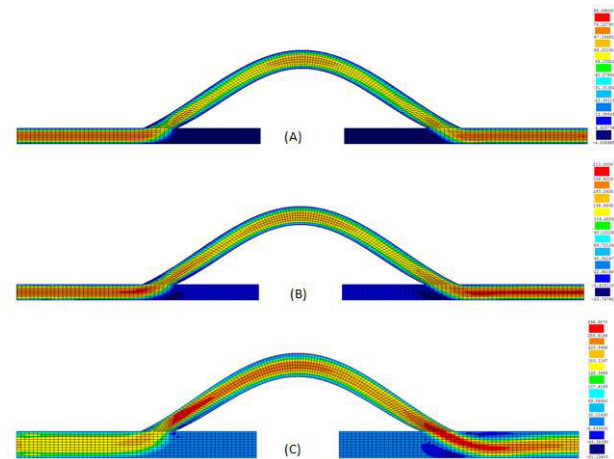

Fig. 3 Longitudinal velocity contours for the graft models A, B and C

Bypasses A and B present maximal velocities inside the host artery before the proximal and just after the distal junctions exhibiting an almost symmetric behavior. As for bypass C the fully developed velocity profile is redirected from the native artery into the graft and velocity reaches its highest value inside the prosthesis just after the proximal anastomosis. The non-symmetric behavior is obvious. Along the distal artery, the flow is gradually stabilized, which is evident from the developing parabolic velocity profile at the outlet. Velocity disturbances are mostly evident in the vicinity of the proximal and distal artery-graft junctions. In these regions, simulations show recirculation and low-velocity zones. Fig. 4 and 5 report particular values for velocities and wall shear stresses (WSS) at positions pointed out in Fig. 2,

such as the geometric location of the end-to-side distal junction and the distal artery floor.
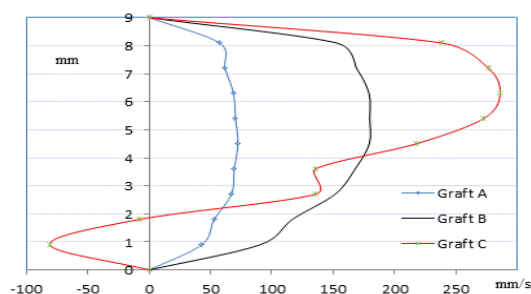

Fig. 4 Longitudinal velocity distributions along distal junction for different models

The velocity behavior along the distal junction of large and narrow grafts is described in Fig. 4. For larger grafts and relatively low velocities, such as simulations A and B, an almost parabolic distribution is reached, no observable velocity reversal, suggesting a low recirculation area formation. On the contrary and for graft C, the development of negative velocities near the floor of the artery indicates separation and flow-reversal zones. The worse graft scenario is for graft C with maximum to peak velocities varying up to 50%. Downstream graft C, the flow demonstrates a strong downwash towards the floor of the native artery, which results in a recirculation zone.

The influence of local hemodynamics on the occurrence of intimal hyperplasia at the distal anastomosis should be investigated considering different associated factors. Beside the occurrence of recirculation and low-velocity zones, it is usually analyzed the distribution of wall shear stress (WSS). Fig. 5 describes the WSS calculated values at the distal artery floor for the three simulated grafts.
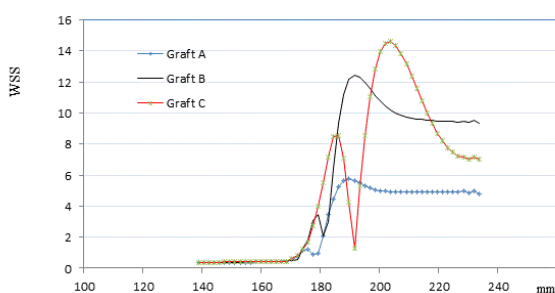

Fig. 5 WSS [Pa] values at the distal artery floor for three different graft models

At the artery floor, the shear stress decreases relatively fast to a zero value, defining a feature that divides the vessel in two regions. Upstream this feature, the presence of a recirculation zone causes a mild WSS value increase. Downstream, the larger

WSS values are due to the strong flow impact on the artery floor. The variability among the WSS plots of grafts B and C demonstrates the flow development in response to the bypass geometry. Graft C presents very large WSS variations associated with high blood impingement at the artery floor on the way out of the graft. As reported by other investigators this area is predominantly susceptible to the occurrence of artery plaque formation diseases [7]. In the distal artery, the presence of stagnant fluid close to the occlusion is the cause for extremely low WSS values in all three considered bypass geometries. Recent patient-specific simulation research of the blood behavior in the systemic arterial tree refers to WSS values varying up to ten Pa, including regions of bends and bifurcations [20]. So, higher values of WSS should be minimized as well as extensive regions of very low values should be avoided towards the optimization of artificial arterial graft geometry.

4 ANN Training

An artificial neural network (ANN) is a mathematical model consisting of a number of highly interconnected processing elements organized into layers with geometry and functionality similar to that of the human brain. The ANN may be regarded as possessing learning capabilities and making it available for later use [22]–[25]. By virtue of its parallel distribution, an ANN is generally robust, tolerant of faults and noise, able to generalize well and capable of solving nonlinear problems. During supervised learning, the ANN is trained on input and target vectors with which it is required to associate an acquired knowledge; thus, with sufficient training, the ANN should be able to perform correctly with previously unseen input vectors.

This project performs an ANN analysis using MATLAB with the Neural Network Application Toolbox (The MathWorks Inc., Natick, MA, USA). The multilayer feed-forward neural network of the software is well suited for function fitting problems. Before beginning the network design process, a sample data set needs to be collected and prepared. Since, it is generally difficult to incorporate prior knowledge into a neural network it can only be as accurate as the used data to train the network. It is important that the data cover the range of inputs for which the network will be used. Multilayer networks can be trained to generalize well within the range of inputs for which they have been trained and it is important that the training data span the full

range of the input space. In the project reported here, a set of 500 input and target vectors has been collected using an FEM simulator within the design space of the four parameters given as follows

$$
\begin{aligned}
10 &\leq \text{H} \leq 40 \text{ mm} \\
0.15 &\leq \beta \leq 0.785 \text{ rad} \\
8 &\leq \text{Wp} \leq 14 \text{ mm} \\
10 &\leq \text{D} \leq 20 \text{ mm}
\end{aligned}
\tag{2}
$$

This was achieved by randomly generating input vectors from the design space established in (2) and running the FEM simulator [11], [14] obtaining the associated target vectors. For the study presented here the simulation was performed using always an artery of 9 mm diameter and prescribing the same boundary conditions at the inlet, a steady parabolic velocity profile of maximum velocity 210 mm/s. Each input vector $\boldsymbol{b}$ has four geometric components $\boldsymbol{b} = (\text{H}, \beta, \text{Wp}, \text{D})$ as described in Fig. 1. Among the simulated results given by the FEM simulator, three functional values qualifying and quantifying the graft local hemodynamics were considered. Each output target vector $\boldsymbol{\varphi} = (\varphi_1, \varphi_2, \varphi_3)$ has been defined with the following components:

$$
\varphi_1(\boldsymbol{b}) = \sum_1^{N_\Gamma} \|WSS\|^2 \tag{3}
$$

where N_Γ is the number of finite element mesh nodes at the floor of the distal artery-graft junction and WSS is the smoothed wall shear stress values given by simulation at the corresponding nodes. The other two components of the output vector are associated with domains of reversed flows. Whenever negative longitudinal velocities are detected in a significant area individual critical domains are assigned contributing to

$$
\varphi_2(\boldsymbol{b}) = \sum_{\Omega_e^*(\boldsymbol{b})} \mathbf{v_x} \tag{4}
$$

being $\mathbf{v_x}$ the elementary longitudinal velocity obtained by using the FEM simulator and $\Omega_e^*(\boldsymbol{b})$ is the reunion of every critical domain of the entire graft artery system. The third component is associated with the particular cross-section $\Omega_{g-a}^*(\boldsymbol{b})$ of the distal graft-artery junction:

$$
\varphi_3(\boldsymbol{b}) = \sum_{\Omega_{g-a}^*(\boldsymbol{b})} \mathbf{v_x}^2 \tag{5}
$$

For the same inlet velocity profile, values of this function $\varphi_3(\boldsymbol{b})$ will be larger for disturbed longitudinal velocity distributions along the distal junction $\Omega_{g-a}^*(\boldsymbol{b})$ and smaller for smooth and parabolic distributions as easily seen by comparing results for grafts B and C shown in Fig. 4.

After the data have been collected, there are two steps that need to be performed before the data are used to train the network, the data need to be pre-processed, and they need to be divided into subsets. A normalization step has been applied to both the input vectors and target vectors of the data set. When training multilayer networks, the general practice is to divide the data into three subsets for training, testing and validation. The considered ratios for training, testing and validation were 0.7, 0.15 and 0.15, respectively. All subsets have been randomly selected within the 500 FEM simulations. The first subset is the training set, which is used for computing the gradient and updating the network weights and biases. The second subset is the validation set. The error on the validation set is monitored during the training process. The validation error normally decreases during the initial phase of training, as does the training set error. However, when the network begins to over-fit the data, the error on the validation set typically begins to rise. The network weights and biases are saved at the minimum of the validation set error.

The feed-forward-net MATLAB call creates a two-layer network with one hidden layer and 10 neurons in the hidden layer. During the configuration step, the number of neurons in the output layer is set to one, which is the number of elements in each vector of targets. The transfer function for hidden layers was the tan-sigmoid transfer function and for the output layer the linear transfer function, often used for function fitting problems. The weights and biases of the network have been initialized with random values and all the training inputs are applied to the network before the weights are updated. Considering a set of input and target data, the mean relative error between target and output results is used to monitor the learning process obtaining the completeness of the modelling. The performance function associated to the process is the mean square error that is the average squared error between the net outputs $\boldsymbol{a}$ and the target outputs $\boldsymbol{t}$. It is defined as follows

$$
mse = \frac{1}{N} \sum_{i=1}^{N} (t_i - a_i)^2 \tag{6}
$$

Either the magnitude of the gradient or the number of validation checks are used to terminate the training. The gradient will become very small as the training reaches a minimum of the performance function. The training stops if the magnitude of the gradient is less than 10^{-5}. The number of validation checks represents the number of successive iterations that the validation performance fails to decrease. If this number reaches 6, the training will

stop. Since the initial weights and biases are randomly set more than one trial was done. The regression analysis was considered using the R value as an indication of the relationship between the outputs and targets. If R = 1, this indicates that there is an exact linear relationship between outputs and targets. If R is close to zero, then there is no linear relationship between outputs and targets. For this example, the training data indicates a good fit. The validation and test results showed R values greater than 0.99. Once the ANN has demonstrated acceptable pattern recognition skills, its creation is complete and it is ready for use.

5 Multi-objective GA

Multiple, often conflicting objectives arise naturally in most real-world optimization scenarios. As evolutionary algorithms possess several characteristics that are desirable for this type of problem, this class of search strategies has been used for multi-objective optimization for more than a decade.

Genetic Algorithms (GAs), a family of biology-inspired methods, are considered here. With a GA a highly effective search of the solution space is performed, allowing a population of strings representing possible solutions to evolve through basic genetic operators. The goal of the genetic operators of the algorithm is to progressively reduce the space design driving the process into more promising regions. GA has many advantages, such as the capability of exploring a large design space, the merit that no gradients information is needed and also it can compute multiple independent objective functions simultaneously in one optimization run. Following the well-known concept of Pareto dominance, optimal solutions, i.e., solutions not dominated by any other solution, may be mapped to different objective vectors. In other words: there may exist several optimal objective vectors representing different trade-offs between the objectives. Therefore, in the following it is assumed that the goal of the optimization is to find or approximate the Pareto set. Accordingly, the outcome of the multi-objective GA is considered to be a set of mutually non-dominated solutions, or Pareto set approximation.

A general multi-objective optimization seeks to optimize the components of a vector-valued objective function mathematically formulated as

$$Minimize \ F(\boldsymbol{b}) = (f_1(\boldsymbol{b}), \cdots, f_m(\boldsymbol{b})) \quad (7)$$

subject to

$$
\begin{aligned}
b_i^{lower} \leq b_i \leq b_i^{upper}, &\quad i = 1, \cdots, n \\
g_k(\boldsymbol{b}) \leq 0 &\quad , \quad k = 1, \cdots, p
\end{aligned}
\quad (8)
$$

where $f_i(\boldsymbol{b})$ is the jth objective function, $\boldsymbol{b} = (b_1, \cdots, b_n)$ is the design variable vector, b_i^{lower} and b_i^{upper} represent the lower and upper boundaries of the ith design variable b_i and $g_k(\boldsymbol{b})$ the kth constraint.

Unlike single objective optimization approaches, the solution to this problem is not a single point, but a family of points known as the Pareto-optimal set. The idea of a solution for (7) with constraints given by (8) can be unclear, because a single point that minimizes all objectives simultaneously usually does not exist. Consequently, the idea of Pareto optimality is used to describe solutions for multi-objective optimization problems. Typically, there are many Pareto optimal solutions for a multi-objective problem. Thus, it is often necessary to incorporate user preferences for various objectives in order to determine a single suitable solution. The weighted sum method for multi-objective optimization problems [26] continues to be used extensively not only to provide multiple solution points by varying the weights consistently, but also to provide a single solution point that reflects preferences presumably incorporated in the selection of a single set of weights [27]. In this work, using the weighted sum method to solve the multi-objective optimization problem entails selecting random scalar weights w_j and minimizing the following composite objective function:

$$\boldsymbol{\phi}(\boldsymbol{b}) = \sum_{j=1}^{m} w_j f_j(\boldsymbol{b}) \quad (9)$$

If all of the weights are positive, as assumed in this study, then minimizing (9) provides a sufficient condition for Pareto optimality, which means that its minimum is always Pareto optimal.

For a shape optimization application, the GA process begins by randomly setting an initial population of possible individuals, where individuals represent different graft geometries. The successive populations maintain the same number of individuals as it evolves throughout successive generations. Each individual is referred as a chromosome containing design variable values referred as genes of the chromosome over which genetic operators are applied. Operators such as selection/crossover, mutation and elimination supported by an elitist strategy are considered to ensure that fitness of the forthcoming generations is always improved [6], [10]. The optimization scheme

includes the following steps:

Initialization, individuals of an initial population are produced randomly each representing a random geometry within the design variable space;

Selection of the progenitors is followed by crossover. The implemented crossover operator builds new individuals using a multipoint combination technique applied over the genes of both selected progenitors;

The implemented mutation is characterized is characterized by two different scenarios: first creating new individuals by swapping a value of a randomly selected variable and secondly by introducing new individuals randomly generated;

Evaluation, fitness of each individual is evaluated using a defined optimization goal and individuals are ranked according to their multi-objective fitness value;

Elimination, deletion of the worst solutions with low fitness simulates the natural death of low fitted individuals. The original size population is recovered and a new population obtained;

Termination checks the termination condition. If it is satisfied, the GA is terminated. Otherwise, the process returns to step Selection/crossover.

Regarding the choice of suitable objective functions for the graft optimization problem, several different approaches have been pursued in the literature. The most frequently considered quantities in the context of blood flow are based on either shear stress or the flow rate. So the previously assigned functions for the ANN output vector will be the vector-valued objective function to minimize. Using positive scalar weights randomly generated, the following composite function

$$\boldsymbol{\phi}(\boldsymbol{b}) = A + \sigma_1\varphi_1(\boldsymbol{b}) - \sigma_2\varphi_2(\boldsymbol{b}) + \sigma_3\varphi_3(\boldsymbol{b}) - P$$
$$\sigma_1 + \sigma_2 + \sigma_3 = 1$$
(10)

is considered for the optimization problem investigated in this work, being A is a positive integer to ensure positiveness and P a value to penalize design vectors that do not conform with the boundary constrains for the geometric design parameters.

Generating the Pareto set can be computationally expensive and is often infeasible, because the complexity of the underlying application prevents exact methods from being applicable. Using the ANN and running the optimization algorithm one hundred times, the obtained Pareto front for this idealized problem is presented in Fig. 6.

For each run of the GA, one set of randomly generated was considered and evolution termination has been defined by fixing the total number of generations as 200. As a compromise between computer time and population diversity, the population and elite group size were taken as 12 and 5, respectively.
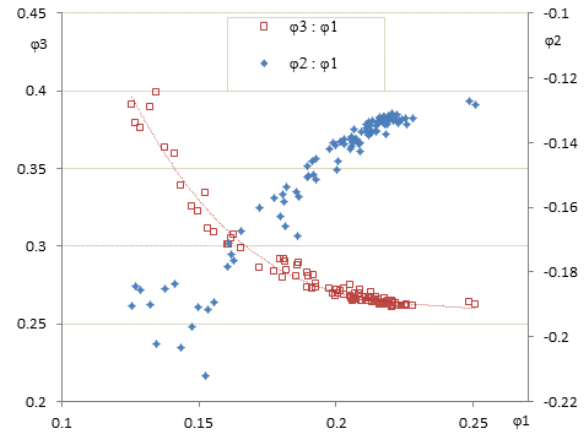

Fig. 6 Pareto front for the multi-objective shape optimization.

6 Optimization Results

Despite deficiencies with respect to depicting the Pareto optimal set, the weighted sum method for multi-objective optimization continues to be used extensively not only to provide multiple solution points by varying the weights consistently, but also to provide single solution points that reflect preferences presumably incorporated in the selection of a single set of weights. For this reason, there is usually no guarantee to identify optimal trade-offs but instead finds good approximations, i.e., a set of solutions whose objective vectors are not too far away from the optimal objective vectors. Details for three bypass grafts extracted from the Pareto front are presented in Table 2 and Fig. 7 to 9.

Table 2. Optimized graft solutions
($V_{peak\ at\ inlet} = 210\ mm/s$).

Optimal solutions	Opt1	Opt2	Opt3
$\varphi 1$	0.249	0.126	0.161
$\varphi 2$	-0.127	-0.191	-0.171
$\varphi 3$	0.264	0.391	0.301
$H_{opt}\ [mm]$	39.899	39.872	28.673
$\beta_{opt}\ [rad]$	0.782	0.237	0.782
$Wp_{opt}\ [mm]$	13.891	8.050	8.114
$D_{opt}\ [mm]$	17.692	16.204	17.406
$V_{min}\ [mm/s]$	-37.	-74.	-40.
$V_{max}[mm/s$	+210.	+270.	+232.

Solution Opt1 corresponds to the graft presenting higher values for the functional $\varphi1$ associated to the WSS values floor of the distal artery-graft junction and lower values for the functional $\varphi3$ associated with the disturbed longitudinal velocity distributions along the distal graft-artery junction. Solution Opt2 corresponds to the opposite conditions and solution Opt3 can be regarded as an intermediate solution establishing a balance between the three considered optimization functions.
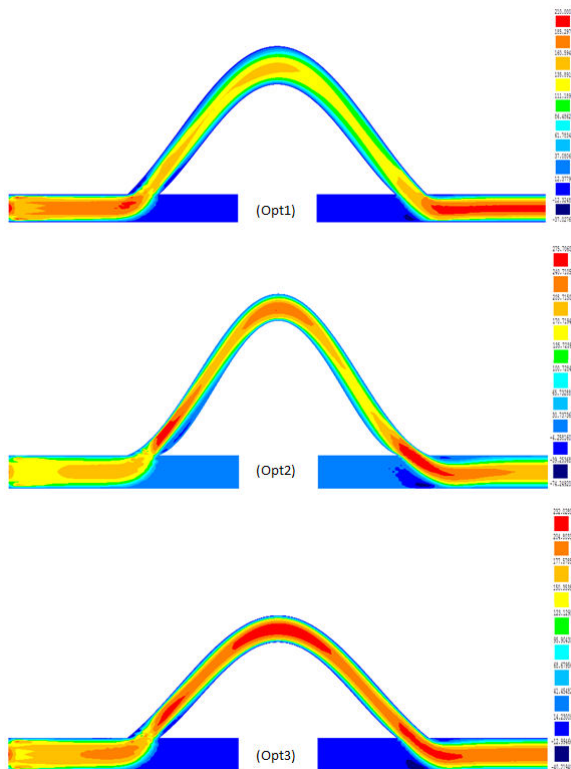

Fig. 7 Velocity contours for three bypass grafts extracted from the Pareto front

Fig. 7 presents the velocity results given in terms of its longitudinal distribution. The velocity contours demonstrate the good quality of the simulations being capable of capturing the flow acceleration as it emerges from the graft to the artery and the flow recirculation at the floor of the host artery, consistently with the expectations. It is interesting to notice that although the abrupt connection between artery and graft induces large velocity variations, the observable reverse flow in grafts Opt1 and Opt3 is quite small. Long residence times usually observable at the distal anastomosis are easily detected in graft Opt2.

Longitudinal velocity distributions along the distal graft-artery junction for the selected optimized grafts are shown in Fig. 8. For larger graft

situations, namely Opt1, an almost parabolic distribution is observed along the whole domain, no observable velocity reversal, suggesting a low recirculation area formation. On the contrary, case graft Opt2, the development of negative velocities near the floor of the artery indicates separation and flow-reversal zones, where extreme values for maximum and minimum velocities are detected.
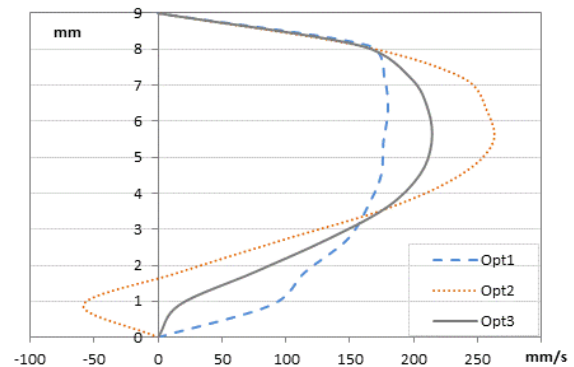

Fig. 8 Longitudinal velocity distributions along the distal junction for selected optimized grafts.

The computed WSS distribution at the floor of the host artery near the distal anastomosis for the selected optimized grafts is reported in Fig. 9.
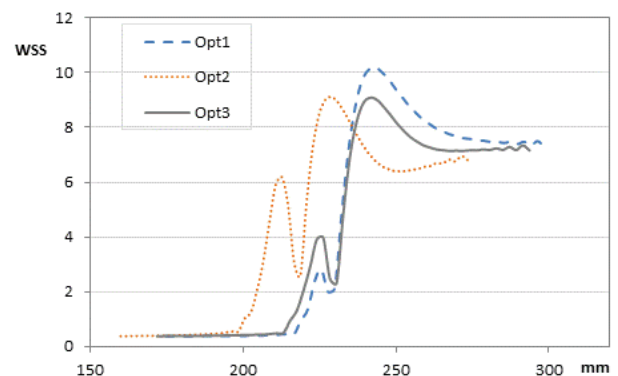

Fig. 9 WSS [Pa] at the artery floor for the selected optimized grafts

As expected, the WSS presents its characteristic variability in the vicinity of the distal junction. Around this region, very large WSS gradients are expected corresponding to the high blood impingement at the artery floor on the way out of the graft. The calculated values of WSS for Grafts Opt1 and Opt3 exhibit smaller gradient as compared to graft Opt2. Those two grafts manage to smooth the blood flow impingement at the artery floor in the way out of the graft. Graft Opt2 presents a larger variation in a smaller region and abnormal shear stresses at the anastomosis might lead to disruption of the arterial anastomosis and false

aneurysm formation. The optimization process manages to achieve geometries presenting WSS values with the expected variability for the blood behavior in the systemic arterial tree [20].

7 Conclusion

The present shape optimization is based on a GA and the objective goal is to reduce the WSS on the floor of the host artery and the oscillatory flows expected at the artery graft junction area. The optimal value for the distance from the near wall of the graft to the near wall of the artery is important but also that the caliber plays an important role in affecting the WSS values at the host artery floor. The choice of optimal parameters comes as a trade-off between WSS values and spatial location of recirculation and long residence times. It can be concluded that geometric parameters might be responsible for the early bypass graft failure.

From this study recommendations to vascular surgeons on how to consider their arterial anastomoses cannot be expected; however future recommendations will be potentially made once, among others, the blood transient nature is accounted for in the optimization process. The study reported herein establishes the methodology as a viable means of achieving optimal artificial graft shapes.

References:
[1] A.M. Imparato, A.Bracco, G.E. Kim and R. Zeff, Intimal and neointimal fibrous proliferation causing failure of arterial reconstruction, *Surgery*, Vol. 72, 1972, pp. 1007-1017.
[2] V.S. Sottiurai, J.S.T. Yao, R.C. Batson, S.L. Sue, R.Jones and Y.A. Nakamura, Distal anastomotic intimal hyperplasia: histopathological character and biogenesis, *Annals of Vascular Surgery*, Vol. 1, 1989, pp. 26–33.
[3] D.P. Giddens, C.K. Zarins and G. S, The role of fluid mechanics in the localization and detection of atherosclerosis, *J. Biomech. Eng.*, Vol.115, 1993, pp. 588-594.
[4] D.N. Ku, D.P. Giddens, C.K. Zarins and S. Glagov, Pulsatile flow and atherosclerosis in the human carotid bifurcation. Positive correlation between plaque location and low oscillating shear stress, *Arteriosclerosis*, Vol. 5 (3), 1985, pp. 293-302.
[5] J.R. Buchanan, C. Kleinstreuer, S. Hyun and G.A. Truskey, Hemodynamics simulation and identification of susceptible sites of atherosclerotic lesion formation in a model abdominal aorta, *Journal of Biomechanics*, Vol. 36, 2003, pp.1185-1196.
[6] C.F. Castro, C.C. António and L.C. Sousa, Multi-objective optimization of bypass grafts in arteries, in *TMSi - Sixth International Conference on Technology and Medical Sciences*, Porto, Portugal, 2010.
[7] C.M. Su, D. Lee, R. Tran-Son-Tay and W. Shyy, Fluid flow structure in arterial bypass anastomosis, *J Biomech Eng.*, Vol. 127 (4), 2005, pp. 611-618.
[8] A. Qiao and Y. Liu, Medical application oriented blood flow simulation, *Clinical Biomechanics*, Vol. 23, 2008, pp. S130–S136.
[9] W. Trubel, H. Schima, A. Moritz, F. Raderer, A. Windisch, R. Ullrich, U. Windberger, U. Losert and P. Polterauer, Compliance mismatch and formation of distal anastomotic intimal hyperplasia in externally stiffened and lumen-adapted venous grafts, *Eur J Vasc Endovac Surg*, Vol. 10, 1995, pp. 415-423.
[10] C.F. Castro, C.C. António and L.C. Sousa, Optimização da geometria do "bypass" arterial, in *Actas do 6º Congresso Luso-Moçambicano de Engenharia*, Maputo, Moçambique, 2011.
[11] L.C. Sousa, C.F. Castro, C.C. António and R. Chaves, Blood flow simulation and vascular reconstruction, Journal of Biomechanics, Vol. 45, 2012, pp. 2549-2555.
[12] J.D. Schaffer, Multi-objective optimization with vector evaluated genetic algorithms, in *Proceedings of the 1st International Conference of Genetic Algorithms*, Pittsburgh, PA, USA, 1985.
[13] A.M. Aragón, J.K. Wayer, P.H. Geubelle, D.E. Goldberg and S.R. White, Design of microvascular flow networks using multi-objective genetic algorithms, *Comput. Methods*

Appl. Mech. Engrg., Vol. 197 (49-50), 2008, pp. 4399–4410.

[14] L. Sousa, C.F. Castro, C.A. Antonio and R. Chaves, Computational Techniques and Validation of Blood Flow Simulation, *WSEAS Transactions on Biology and Biomedicine*, Included in ISI/SCI Web of Science and Web of Knowledge, Vol. 4-8, 2011, pp. 145-155.

[15] M. Probst, M. Lülfesmann, M. Nicolai, H.M. Bücker, M. Behr and C.H. Bischof, Sensitivity of optimal shapes of artificial grafts with respect to flow parameters, *Comput. Methods Appl. Mech. Engrg.*, Vol. 199, 2010, pp.997-1005.

[16] M. Probst, M. Lülfesmann, H.M. Bücker, M. Behr and C H. Bischof, Sensitivity of shear rate in artificial grafts using automatic differentiation, *Int. J. Numer. Meth. Fluids*, Vol. 62, 2010, pp. 1047-1062.

[17] K. Perktold, M. Hofer, G. Karner, W. Trubel and H. Schima, Computer simulation of vascular fluid dynamics and mass transport: *Optimal design of arterial bypass anastomoses, in ECCOMAS 98*, Athens, Greece, 1998.

[18] D. Fei, J.D. Thomas and S.E. Rittgers, The effect of angle and flow rate upon hemodynamics in distal vascular graft anastomoses: A numerical model study, *ASME Journal of Biomedical Engineering*, Vol. 116, 1994, pp. 331-336.

[19] K. Perktold, M. Resch and F.H., Pulsatile Non-Newtonian Flow Characteristics in a Three-Dimensional Human Carotid Bifurcation Model, *ASME J. Biomech. Eng.*, Vol. 113, 1991, pp. 463–475.

[20] P. Reymond, F. Perren, F. Lazeyras and N. Stergiopulos, Patient-specific mean pressure drop in the systemic arterial tree, a comparison between 1-D and 3-D models, *Journal of Biomechanics*, Vol. 45, 2012, pp. 2499-2505.

[21] H.S. Bassiouny, S. White, S. Glagov, E. Choi, D.P. Giddens and C.K. Zarins, Anastomotic intimal hyperplasia: mechanical injury or flow induced, *J. Vas. Surg.*, Vol. 15, 1992, pp. 708-716.

[22] R. Beale and T. Jackson, *Neural Computing: An Introduction*, Bristol, U.K.: IOP Publishing Ltd., 1990.

[23] S.S. Cross, R.F. Harrison and R.L. Kennedy, Introduction to neural networks, *The Lancet*, Vol. 346(8982), 1995, pp.1075-1079.

[24] S. Haykin, *Neural networks: A comprehensive foundation*, New York: Macmillan, 1994.

[25] D.R. Hush and B.G. Horne, Progress in supervised neural networks, *IEEE Signal Proc. Magazine*, Vol. 10(1), 1993, pp. 8-39.

[26] R.L. Marler and J.S. Arora, The weighted sum method for multi-objective optimization: new insights, *Structural and Multidisciplinary Optimization*, Vol. 41(6), 2010, pp. 853-862.

[27] M. Poursina, C.A.C António, C.F. Castro, J. Parvizian and L.C. Sousa, Preform optimal design in metal forging using genetic algorithms, *Engineering Computations (Swansea, Wales)*, Vol. 21(6), 2004, pp. 631-650.